# Attosecond photoemission dynamics encoded in real-valued continuum wave functions

Romain Gaillac,[1,2] Morgane Vacher,[1,3] Alfred Maquet,[1] Richard Taïeb,[1] and Jérémie Caillat[1]

[1]*Sorbonne Universités, UPMC Univ. Paris 06, CNRS, UMR 7614, Laboratoire de Chimie Physique–Matière et Rayonnement, F-75005 Paris, France*

[2]*Department of Chemistry, École Normale Supérieure, 24, rue Lhomond, 75005 Paris, France*

[3]*Department of Chemistry, Imperial College London, London SW7 2AZ, United Kingdom*

(Received 17 February 2015; published 14 January 2016)

The dynamics of photoemission is fully encoded in the continuum wave functions selected by the transitions. Using numerical simulations on simple benchmark models, we show how scattering phase shifts and photoemission delays can be retrieved from this unambiguously defined class of wave functions. In contrast with standard scattering waves inherited from collision theory, they are real-valued for one-photon transitions and provide a clear-cut interpretation of the delays recently discussed in the framework of attosecond science.

DOI: 10.1103/PhysRevA.93.013410

## I. INTRODUCTION

The advent of attosecond science, with its main objectives of probing and controlling ultrafast dynamics in quantum systems [1–5], has recently brought about a fresh view of photoemission. This very fundamental process was indeed recently revisited in the time domain, in a series of pioneering experiments [6–9] that were soon accompanied by intense theoretical activity devoted to the interpretation of the reported "photoemission delays"; see, e.g., [10–19].

Theory has established that the dynamics intrinsic to photoemission reduces to electron scattering dynamics. It reflects the influence of the parent ionic potential on photoelectron motion as compared to a reference motion (typically in the universal long-range Coulomb potential). From the point of view of quantum mechanics, it is imprinted in the phase of the photoelectron wave function, e.g., through the concept of group delay [20,21]. Nevertheless, the simplicity of the underlying physics is not fully recognized. This is partly due to the complexity of the analyses used to retrieve such delays out of currently available experimental pump-probe measurements, which focus the discussion on the influence of the probe on the measured values. From a theoretical viewpoint, one may attribute the difficulties of interpretation to the standard formalism used to describe the photoemission continuum. The latter is commonly expanded on the basis of complex-valued incoming scattering wave functions, inherited from the S-matrix formalism of collision theory [22]. In this framework, the scattering phase related to photoemission appears as the argument of the *dipole transition amplitude*, thus obscuring the significance of the associated group delay. It is not unusual, for example, that the photoemission delays are misinterpreted as "the time it takes to absorb a photon."

In this article, we present the benefits of working directly with the continuum wave functions *selected* by the transitions, reminiscent of the so-called eigenchannel wave functions [23]. This original formalism provides a direct and transparent interpretation, notably in terms of dynamics, and restores simplicity to a process as elementary as photoemission.

## II. SELECTED CONTINUUM WAVE FUNCTIONS

The selected continuum wave functions (SCWFs) are solutions of the time-independent Schrödinger equation (TISE), which (i) carry all the information related to the continuum reached upon photoionization, (ii) are defined unambiguously, irrespective of the arbitrary basis with which one chooses to work, and (iii) are real-valued for single-photon transitions [24].

For a single-photon transition from a bound state $|\psi_{\rm ini}\rangle$, with energy $E_{\rm ini}$, toward the continuum at energy $E$, the selected continuum state is defined in the framework of first-order perturbation theory as

$$|\phi_{E,\rm sel}\rangle = \sum\!\!\!\!\!\!\int_{\nu} \langle\phi_{E,\nu}|\hat{\rm d}|\psi_{\rm ini}\rangle\,|\phi_{E,\nu}\rangle, \tag{1}$$

where $\hat{\rm d}$ is the dipole operator accounting for the electron(s) interaction with the electric field. This definition makes use of an *arbitrary* orthonormal eigenbasis $\{|\phi_{E,\nu}\rangle\}$, spanned by the (multi-)index $\nu$, for the degenerate continuum reached at energy $E$. Note that the sum/integral in Eq. (1) is restricted to a subspace at a well-defined specific energy: it should not be mistaken for the closure relation for the complete space of the system's quantum states. As long as the expansion is complete for the manifold of interest, the above defined selected state carries all possible information on the transition—including its dynamics. As developed below, the scattering phase shift characterizes the asymptotic oscillations of the SCWF associated with $|\phi_{E,\rm sel}\rangle$, in comparison with an arbitrary reference wave to be specified.

In the following, we illustrate the simplicity of interpretation allowed by the SCWF, with a series of numerical experiments performed on one-dimensional (1D) and 3D model systems with a focus on ionization timing. Our approach consists in comparing the photoemission dynamics inferred from the analysis of the stationary SCWF to the one directly revealed in a time-dependent treatment (as, e.g., in [13,25]), following the line of reasoning established by Wigner in the context of collisions [20]. The two aspects are formally linked by expressing the time-dependent electron wave packet (EWP) as the coherent spectral superposition

$$|\psi_{\rm EWP}(t)\rangle = \int F(\omega)|\phi_{E,\rm sel}\rangle e^{-iEt/\hbar}\,dE \tag{2}$$

 

of the SCWFs over the energy range covered by the ionizing pulse, with $F(\omega)$ being the field's spectral amplitude at frequency $\omega = (E - E_{\rm ini})/\hbar$ [26].

It is mandatory to consider the complete spectral and temporal profiles when dealing with structured wave packets, e.g., formed in the vicinity of autoionizing states or narrow shape resonances. Here, we considered for simplicity processes producing continuum EWP unstructured enough to have their dynamics properly characterized by group delays—as notably assumed in most of the studies on the topic of time-resolved photoemission so far. After introducing the numerical tools used in this work, we present the results obtained for three different benchmark systems, with an emphasis on photoemission anisotropy resulting either from the intrinsic anisotropy of the potential, or from the asymmetry of the initial state. This last issue was recently addressed from the perspective of "streaking" measurements [27,28].

## III. SIMULATIONS

### A. Numerical toolbox

We simulated the "exact" photoemission dynamics of the model systems interacting with (unchirped) xuv light pulses by solving the time dependent Schrödinger equation numerically with standard algorithms [29]. We characterized it through a flux analysis of the time-dependent wave function by defining a numerical "time of flight" ($\bar{t}$) toward a virtual detector as

$$\bar{t}(\vec{r}_{\rm d}) = \frac{\int t \times \vec{j}(\vec{r}_{\rm d},t)\cdot\vec{n}\,dt}{\int \vec{j}(\vec{r}_{\rm d},t)\cdot\vec{n}\,dt}, \tag{3}$$

where $\vec{j}(\vec{r}_{\rm d},t)\cdot\vec{n}$ is the outgoing electron flux computed at the detection position $\vec{r}_{\rm d}$ along the direction $\vec{n} = \frac{\vec{r}_{\rm d}}{|\vec{r}_{\rm d}|}$. As mentioned in the Introduction, there is no absolute "ionization time": the time of flight computed for each photoemission event must be compared to a reference one, $\bar{t}_{\rm ref}$. While their values obviously depend on the detection position $\vec{r}_{\rm d}$, their difference

$$\Delta\bar{t} = \bar{t}(\vec{r}_{\rm d}) - \bar{t}_{\rm ref}(\vec{r}_{\rm d}) \tag{4}$$

is constant as long as the fluxes are computed in the asymptotic region, where the ionic potential and the reference one coincide. Another condition for the stability of $\Delta\bar{t}$ is that the fluxes display smooth, bell-shaped, temporal profiles. This was ensured by using spectrally narrow xuv pulses (their durations were set to ∼50 fs) and detection distances $|\vec{r}_{\rm d}|$ short enough to prevent significant spreading of the EWP. To compare $\Delta\bar{t}$ to group delays inferred from time-independent wave functions, each EWP must also be assigned a representative energy. We chose the average photoelectron energy,

$$\bar{E} = \frac{\int E \times \sigma(E)\,dE}{\int \sigma(E)\,dE}, \tag{5}$$

where $\sigma(E)$ is the photoelectron spectrum at energy $E$, computed in our simulations with the window technique [30].

We now turn to the time-independent approach, i.e., the analysis of the SCWF associated with the considered transitions. The general idea is to associate a group delay with the asymptotic phase shift of the SCWF at a given energy $E$, $\phi_{E,\rm sel}$, compared to the chosen reference wave function at the same energy, $\phi_{E,\rm ref}$. In practice, the phase shift can be computed as [31]

$$\eta(E) = -\arctan\frac{W[\phi_{E,\rm sel};\phi_{E,\rm ref}]|_{\vec{r}_{\rm d}}}{W[\phi_{E,\rm sel};\phi_{E,\rm cpl}]|_{\vec{r}_{\rm d}}}, \tag{6}$$

where $W[f;g] = f'g - g'f$ is the radial Wronskian functional [32], involving the wave-function derivatives along $\vec{n}$. The computation of $\eta(E)$ implies an additional ("complementary") wave function of the reference system, $\phi_{E,\rm cpl}(\vec{r})$, orthogonal to $\phi_{E,\rm ref}(\vec{r})$ along the radial coordinate. The scattering group delay [20] associated with photoemission at the particular energy $\bar{E}$ is then defined as

$$\tau = \hbar\frac{\partial\eta(E)}{\partial E}\bigg|_{\bar{E}}. \tag{7}$$

For three different model systems, we now compare the delays $\Delta\bar{t}$, as evaluated in the time-dependent simulations according to Eq. (4), to the group delays $\tau$ inferred from the time-independent SCWF according to Eq. (7).

### B. Photoionization of a symmetric model atom

We start with a model atom made of a single 1D "electron" in a symmetric potential $V_1(x)$ built on a soft-Coulomb term $V_0(x)$ augmented with short-range hyper-Gaussian barriers [13], as represented in Fig. 1 (black full curve). The short-range barriers are designed to affect significantly the electron dynamics in the near-threshold continuum. They are notably responsible for a shape resonance of energy $E_{\rm R} = 1.86$ eV and width $\Gamma_{\rm R} = 0.39$ eV, corresponding to a lifetime $\tau_{\rm R} = 1.71$ fs—much shorter than the simulated pulse durations. We considered photoemission with xuv central energies $\hbar\omega$ in the range 16.5–18.5 eV, reaching the vicinity of $E_{\rm R}$. We took as a reference the companion model atom with the potential restricted to the long-range term $V_0(x)$. The initial state is the ground state ($|\psi_{\rm ini}\rangle = |\psi_0\rangle$), with energy $E_0 = -15.64$ eV for both potentials.

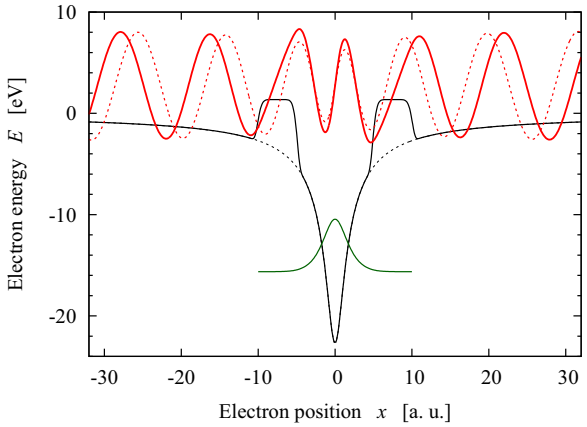


FIG. 1. Symmetric 1D potential $V_1(x)$ (black full curve) and reference potential $V_0(x)$ (dashed black curve). Real-valued continuum wave functions at $E = 2.72$ eV (unnormalized): selected wave function $\phi_{E,\rm sel}(x)$ associated with $V_1(x)$ (full red curve) and reference wave function $\phi_{E,\rm ref}(x)$ (dotted red curve). The initial state is the ground state (green full curve, practically identical for the two systems).

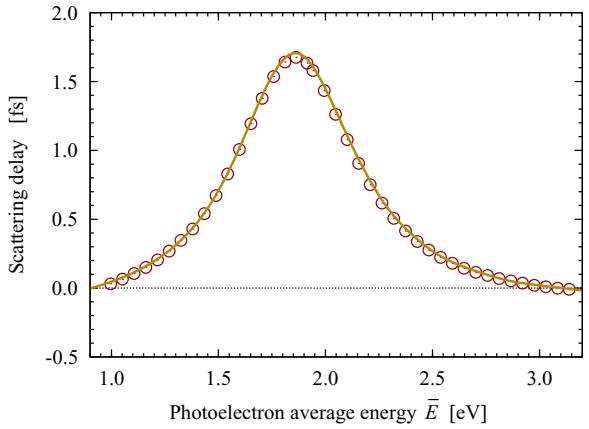


FIG. 2. Delays in photoemission of the symmetric 1D model atom from its ground state, as a function of the average photoelectron energy $\bar{E}$: $\Delta\bar{t}$ (circles); $\tau$ (full curve). The reference is photoemission from the soft-Coulomb potential.

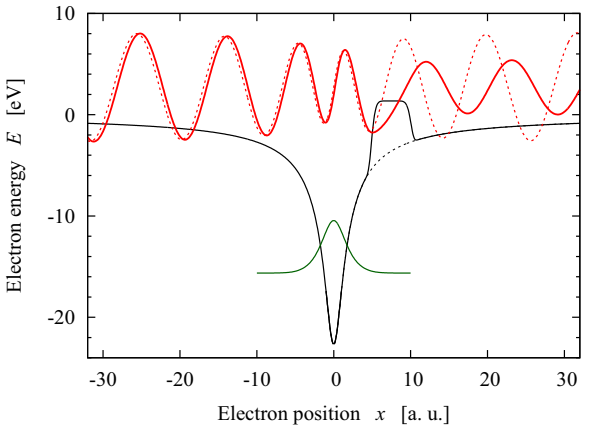


FIG. 3. Same as Fig. 1, but for the asymmetric model system with potential $V_2(x)$ (black curve).

Computing the continuum wave functions needed to evaluate the phase shift $\eta(E)$ [Eq. (6)] is straightforward in this case, since we start from a symmetric initial state: The 1D selection rule imposes $\phi_{E,\mathrm{sel}}(x)$ and $\phi_{E,\mathrm{ref}}(x)$ to be antisymmetric in $x$. The complementary function $\phi_{E,\mathrm{cpl}}(x)$ is consequently symmetric. All functions were computed using a Runge-Kutta algorithm [29] with symmetry-adapted initial conditions at $x = 0$. The functions $\phi_{E,\mathrm{sel}}(x)$ and $\phi_{E,\mathrm{ref}}(x)$ obtained at an illustrative energy $E = 2.72$ eV are shown in Fig. 1 (full and dotted red curves, respectively), displaying a clear relative phase shift accumulated under the barriers.

We reported in Fig. 2 the delays evaluated as $\Delta\bar{t}$ [Eq. (4)] and $\tau$ [Eq. (7)] against the mean photoelectron energy $\bar{E}$. Unsurprisingly, the two sets of data follow a bell-shaped curve centered at the resonant energy $\bar{E} = E_{\mathrm{R}}$, with a maximum value equal to the lifetime $\tau_{\mathrm{R}}$ and a width governed by $\Gamma_{\mathrm{R}}$. They are in excellent agreement.

This first example illustrates in a symmetrical case how dynamical properties of photoemission are imprinted in the real-valued SCWFs. In the following, we investigate anisotropic photoemission resulting from an anisotropic potential and/or initial state. Although we consider again simple cases, they constitute benchmark systems to address anisotropic molecular photoemission.

### C. Photoionization of an asymmetric model system

The second model is an asymmetric 1D system with a potential $V_2(x)$ derived from the first one, where a barrier is located on the *right side* only ($x > 0$); see Fig. 3 (full black curve). We simulated photoemission from its ground state with xuv central energies $\hbar\omega$ ranging from 18 to 36 eV. We characterized the anisotropic photoemission by comparing electron ejection toward the right ($x \to +\infty$) and the left ($x \to -\infty$) sides of the "molecule."

The delays $\Delta\bar{t}$ were computed here as the difference between the times of flight obtained at $x_{\mathrm{d}} > 0$ on the one hand, and at $-x_{\mathrm{d}}$ on the other hand, i.e., according to Eq. (4) with $\bar{t}_{\mathrm{ref}}(x_{\mathrm{d}}) = \bar{t}(-x_{\mathrm{d}})$.

The obtention of the stationary continuum wave functions is not as straightforward as before, since the selection rule no longer applies to asymmetric systems. One has to refer to the definition of the SCWF [Eq. (1)], which transposed here reads

$$\phi_{E,\mathrm{sel}}(x) = \sum_{\nu=1,2} \langle \phi_{E,\nu} | \hat{\mathrm{x}} | \psi_0 \rangle \, \phi_{E,\nu}(x), \tag{8}$$

since the continuum in one dimension is doubly degenerate. The arbitrary orthonormal eigenbasis $\{\phi_{E,1}(x), \phi_{E,2}(x)\}$ was computed by solving the TISE at each continuum energy $E$ for a set of intermediate functions, using the Runge-Kutta propagator (toward the right and the left) with different conditions at the origin, followed by a Gram-Schmidt orthonormalization.

The SCWF $\phi_{E,\mathrm{sel}}(x)$ obtained for the energy $E = 2.72$ eV is displayed in Fig. 3 (full red curve). The anisotropy of photoemission is clearly reflected in the asymmetry of its asymptotic phases and amplitudes.

To evaluate the left-to-right phase shift, we used an intermediate reference, which is again photoemission from the potential $V_0(x)$. The intermediate reference wave function, $\phi_{E,\mathrm{ref}}(x)$, is also shown in Fig. 3 (dotted red curve), identical to the one displayed in Fig. 1. As could be expected, the selected and reference wave functions, $\phi_{E,\mathrm{sel}}(x)$ and $\phi_{E,\mathrm{ref}}(x)$, are almost in phase on the left side ($x < 0$), where the potentials are equal, while a pronounced phase shift accumulated under the barrier shows up on the right side ($x > 0$).

We computed the related intermediate phase shifts $\eta_{\mathrm{right}}(E)$ and $\eta_{\mathrm{left}}(E)$, using Eq. (6) at the positions $x_{\mathrm{d}}$ and $-x_{\mathrm{d}}$, respectively, and the same $\phi_{E,\mathrm{ref}}(x)$ and $\phi_{E,\mathrm{cpl}}(x)$ as in Sec. III B. The phase shift accounting for the asymmetric photoemission is thus

$$\eta(E) = \eta_{\mathrm{right}}(E) - \eta_{\mathrm{left}}(E). \tag{9}$$

Figure 4 shows the delays $\Delta\bar{t}$ [Eq. (4)] as well as the group delays $\tau$ derived from $\eta(E)$ [Eqs. (7) and (9)] as a function of $\bar{E}$. The asymmetry of the potential results in "stereo" photoemission delays [27] evolving between $-100$ and $+250$ as. The delays are much shorter and their spectral variations much broader than with the symmetric model, where the electron could be resonantly "trapped" between the two barriers. Here as well, the excellent agreement between

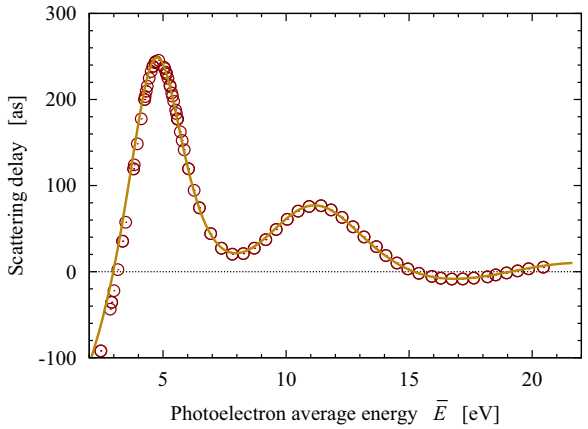


FIG. 4. Delays in photoemission of the asymmetric 1D model molecule from its ground state, as a function of the average photoelectron energy $\bar{E}$: $\Delta\bar{t}$ (circles); $\tau$ (full curve). Here, the delays characterize photoemission toward the right as compared to the left.

the two sets of data validates the characterization of the photoemission dynamics by means of a group delay, derived from a straightforward interpretation of the SCWF.

### D. Photoionization of $He^+(2p_0)$

As a last example, we treat photoemission from $He^+$ initially in its $2p_0$ state. The anisotropy is no longer related to the potential, which is spherically symmetric, but only to the shape of the initial state. The purpose is to show how the SCWF analysis applies to 3D systems, using the standard selection rules inherent to the partial wave representation of wave functions. In addition, we used the analytic solutions available for hydrogenic ions to cross-check the results obtained numerically.

We consider photoemission by a linearly polarized pulse of central energy $\hbar\omega = 17.06$ eV, generating photoelectrons with an average energy $\bar{E} = 3.46$ eV. We characterized the anisotropic photoemission by evaluating angularly resolved delays, taking photoemission along the laser polarization direction as a reference ($\theta_{\rm ref} = 0, \varphi_{\rm ref} = 0$). Due to the conserved cylindrical symmetry around $z$, the analysis is actually restricted to the $zx$ plane ($\varphi = 0$). The orientation-dependent delays $\Delta\bar{t}(\theta_{\rm d})$ were computed according to Eq. (4) by comparing the time of flight toward the detector position $\vec{r}_{\rm d} = (r_{\rm d}, \theta_{\rm d}, 0)$ to the one obtained along $z$ at the same distance: $\bar{t}_{\rm ref}(r_{\rm d}, \theta_{\rm d}) = \bar{t}(r_{\rm d}, 0)$.

The selection rule $\Delta\ell = \pm 1$ was exploited to compute the SCWF using a compact partial-wave expansion as

$$\phi_{E,\rm sel}(r,\theta,\varphi) = \sum_{\ell=0,2} c_\ell \; R_{E\ell}(r) \; Y_{\ell 0}(\theta,\varphi), \qquad (10)$$

where the functions $R_{E\ell}(r)$ are normalized, real-valued, regular continuum solutions of the radial TISE [33] and $c_\ell = \langle R_{E\ell} Y_{\ell 0} | z | R_{2p} Y_{10} \rangle$. A cut of $\phi_{\bar{E},\rm sel}$ in the $zx$ plane is shown in Fig. 5(a). The overall wave function is clearly dominated by its $d$ component ($|c_2/c_0| \approx 3.29$)—displaying a $\sigma_g$ symmetry and an angular change of sign around the "magic" angle $\theta_{\rm c} \simeq 54.7°$—blurred by the $s$ contribution. The interplay

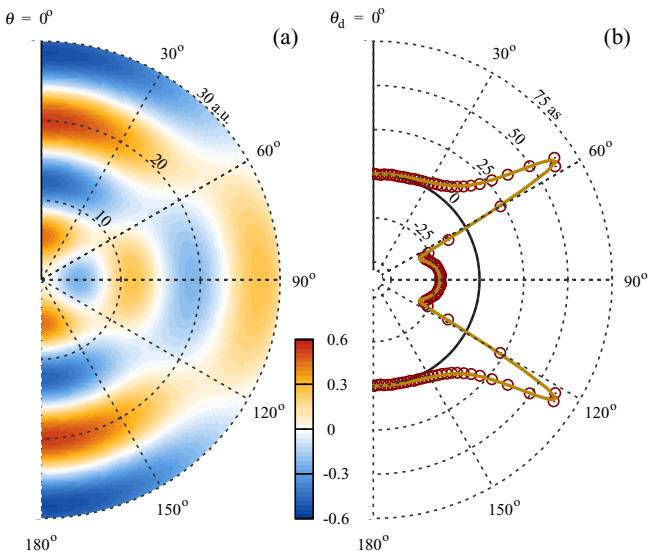


FIG. 5. Photoionization of $He^+(2p_0)$ by a pulse of central energy $\hbar\omega = 17.06$ eV. (a) Real-valued continuum wave function selected by the one-photon transition at $E = 3.46$ eV (cut in the $zx$ plane). (b) Ionization delays against the electron detection direction $\theta_{\rm d}$: $\Delta\bar{t}$ (circles); $\tau$ (full curve). Here, the delays are defined and computed at each orientation by taking photoemission along $\theta_{\rm d} = 0$ as a reference.

between the $s$ and $d$ components results in angular variations of the SCWF asymptotic phase.

We computed *intermediate* phase shifts, $\eta_{\rm int}(E,\theta_{\rm d})$, according to Eq. (6) using the regular and irregular $s$ partial waves as an arbitrary reference and complementary functions, respectively. We then evaluated the orientation-dependent group delay $\tau$ at the average photoelectron energy $\bar{E}$ from the phase shift of interest,

$$\eta(E,\theta_{\rm d}) = \eta_{\rm int}(E,\theta_{\rm d}) - \eta_{\rm int}(E,0), \qquad (11)$$

according to Eq. (7).

We plotted $\Delta\bar{t}$ and $\tau$ against the detection direction $\theta_{\rm d}$ in Fig. 5(b). Following a pattern reproducing the symmetries of the SCWF, the delays range from $-20$ to $+60$ as with very fast angular variations between 30° and 60° (first quadrant)—a reminiscence of the strong variations of the $d/s$–wave-amplitude ratio around $\theta_{\rm c}$. Here as well, the two sets of data are in excellent agreement. The same results were obtained when taking, for example, the $d$ waves as arbitrary references to compute the intermediate phase shifts $\eta_{\rm int}$. Note that the delays evidenced here are expressed in attoseconds: This is the natural time scale for photoelectron dynamics in smooth continua, far from the influence of any quasibound states [8,9].

With this last example, we want to emphasize the completeness of the information encoded in the selected wave function, more precisely in the anisotropic phases *and* amplitudes of its asymptotic oscillations (see Fig. 5). While the phase shifts are directly related to the ionization dynamics as discussed above, the asymptotic amplitudes can be used to retrieve the

photoelectron angular distribution as

$$\rho(\theta,\varphi) = \int_{s_a}^{s_a+2\pi} |\phi_{E,\mathrm{sel}}(r,\theta,\varphi)|^2 \, ds, \tag{12}$$

where $s = kr - Z/k \log(2kr)$ encompasses all the $r$-dependent contributions to the phase of the oscillating SCWF at a given orientation $(\theta,\varphi)$ [32], $k = \sqrt{2m_e E}/\hbar$ is the wave number associated with the continuum energy $E$, $Z$ corresponds to the ionic charge in the final state, and the integration end point $s_a$ lies in the asymptotic region. In the case treated here, the partial-wave expansion [Eq. (10)] and the asymptotic behavior of the radial functions,

$$\lim_{r\to\infty} R_{E,\ell}(r) \propto \sin(s - \ell\pi/2 + \sigma_\ell), \tag{13}$$

where $\sigma_\ell = \arg\Gamma(\ell + 1 - iZ/k)$ is the $r$-independent Coulomb phase shift [32], provide an analytic expression for $\rho(\theta,\varphi)$,

$$\begin{aligned}\rho(\theta,\varphi) \propto{}& c_0^2 Y_{00}^2(\theta,\varphi) \int_{s_a}^{s_a+2\pi} \sin^2(s+\sigma_0)\, ds \\ &+ c_2^2 Y_{20}^2(\theta,\varphi) \int_{s_a}^{s_a+2\pi} \sin^2(s+\sigma_2)\, ds \\ &- 2c_0c_2 Y_{00}(\theta,\varphi) Y_{20}(\theta,\varphi) \\ &\times \int_{s_a}^{s_a+2\pi} \sin(s+\sigma_0)\sin(s+\sigma_2)\, ds \\ \propto{}& \pi\big[c_0^2 Y_{00}^2(\theta,\varphi) + c_2^2 Y_{20}^2(\theta,\varphi) \\ &- 2c_0c_2 Y_{00}(\theta,\varphi) Y_{20}(\theta,\varphi)\cos(\sigma_2-\sigma_0)\big],\end{aligned} \tag{14}$$

which is, indeed, the well-established distribution [34] obtained using conventional scattering functions (up to a normalization constant). We have verified numerically that a similar analysis could be applied to the photoemission from the asymmetric 1D model considered in Sec. III C (results not shown).

## IV. CONCLUSION

In this article, we have shown how ionization dynamics are encrypted in the continuum wave functions *selected* by the transitions, in comparisons with the temporal profiles revealed in time-dependent simulations. For simplicity, we have considered situations in which group delays are relevant quantities to characterize the dynamics of photoemission. We notably illustrated how the SCWFs encode the anisotropy of photoemission inherited from the potential and/or from the initial-state asymmetry.

The interpretation of the SCWF asymptotic phase shifts in terms of group delays with the standard tools of wave mechanics [21] is transparent, and it highlights the necessity to specify a reference when defining a delay. This is particularly important in the analysis of experimental measurements, where handling the reference issue is in general not straightforward. Furthermore, an analysis centered on real-valued SCWFs highlights the fact that, in one-photon transitions, ionization delays are related solely to electron scattering by the ionic core potential, rather than to a hypothetical transition duration.

The methodology exposed in these benchmark studies can be directly extended to investigate photoemission dynamics from molecules, with the usual limitations inherent to the computational treatment of low-symmetry, many-body problems [22,35]. The phase shifts then carry all the information concerning the released electron interaction with the remaining core, including the correlation with the other electrons [36–38].

Finally, for higher-order processes, the transition operator will make the SCWF *complex* valued as soon as an intermediate resonance contributes to the transition [39]. The additional phase factor carried by the SCWF can then be interpreted in terms of a *transition* delay [7,13,40,41].

## ACKNOWLEDGMENTS

The authors acknowledge passionate and stimulating discussions with Marcus Dahlström and Stefan Haessler. This project is supported by French state funds managed by the Agence Nationale de la Recherche programme ANR-09-BLAN-0031-01ATTO-WAVE and ANR Investissements d'Avenir ANR-11-IDEX-0004-02.

[1] 10th anniversary of attosecond pulse generation, special issue edited by R. Kienberger, Z. Chang, and C. H. Nam, J. Phys. B **45** (2012).

[2] Attosecond photonics focus issue, Nat. Photon. **8**, 161–264 (2014).

[3] *Attosecond Physics*, edited by L. Plaja *et al.*, Springer Series in Optical Science Vol. 177 (Springer-Verlag, Berlin, 2013).

[4] S. Leone *et al.*, What will it take to observe processes in "real time"? Nat. Photon. **8**, 162 (2014).

[5] L.-Y. Peng *et al.*, Tracing and controlling electronic dynamics in atoms and molecules by attosecond pulses, Phys. Rep. **575**, 1 (2015).

[6] A. L. Cavalieri *et al.*, Attosecond spectroscopy in condensed matter, Nature (London) **449**, 1029 (2007).

[7] S. Haessler *et al.*, Phase-resolved attosecond near-threshold photoionization of molecular nitrogen, Phys. Rev. A **80**, 011404 (2009).

[8] M. Schultze *et al.*, Delay in photoemission, Science **328**, 1658 (2010).

[9] K. Klünder *et al.*, Probing Single-Photon Ionization on the Attosecond Time Scale, Phys. Rev. Lett. **106**, 143002 (2011).

[10] A. S. Kheifets and I. A. Ivanov, Delay in Atomic Photoionization, Phys. Rev. Lett. **105**, 233002 (2010).

[11] M. Ivanov and O. Smirnova, How Accurate is the Attosecond Streak Camera? Phys. Rev. Lett. **107**, 213605 (2011).
[12] C.-H. Zhang and U. Thumm, Streaking and Wigner time delays in photoemission from atoms and surfaces, Phys. Rev. A **84**, 033401 (2011).
[13] J. Caillat, A. Maquet, S. Haessler, B. Fabre, T. Ruchon, P. Salieres, Y. Mairesse, and R. Taieb, Attosecond Resolved Electron Release in Two-Color Near-Threshold Photoionization of $N_2$, Phys. Rev. Lett. **106**, 093002 (2011).
[14] S. Nagele *et al.*, Time-resolved photoemission by attosecond streaking: Extraction of time information, J. Phys. B **44**, 081001 (2011).
[15] J. M. Dahlström, A. L'Huillier, and A. Maquet, Introduction to attosecond delays in photoionization, J. Phys. B **45**, 183001 (2012).
[16] G. Dixit, H. S. Chakraborty, and M. E.-A. Madjet, Time Delay in the Recoiling Valence Photoemission of Ar Endohedrally Confined in $C_{60}$, Phys. Rev. Lett. **111**, 203003 (2013).
[17] A. Maquet, J. Caillat, and R. Taïeb, Attosecond delays in photoionization: Time *and* quantum mechanics, J. Phys. B **47**, 204004 (2014).
[18] J. M. Dahlström, M. Vacher, A. Maquet, J. Caillat, and S. Haessler, Photoionization time delays, in *Ultrafast Dynamics Driven by Intense Light Pulses*, edited by M. Kitzler and S. Gräfe, Springer Series in Atomic, Optical, and Plasma Physics Vol. 86 (Springer, Switzerland, 2016), pp. 177–202.
[19] R. Pazourek, S. Nagele, and J. Burgdörfer, Attosecond chronoscopy of photoemission, Rev. Mod. Phys. **87**, 765 (2015).
[20] E. P. Wigner, Lower limit for the energy derivative of the scattering phase shift, Phys. Rev. **98**, 145 (1955).
[21] D. J. Tannor, *Introduction to Quantum Mechanics: A Time-Dependent Perspective*, 1st ed. (University Science Books, Sausalito, CA, 2007).
[22] A. F. Starace, Theory of atomic photoionization, in *Encyclopedia of Physics*, edited by S. Flügge and W. Mehlhorn (Springer-Verlag, Berlin, 1982), pp. 7–23.
[23] D. Loomba, S. Wallace, D. Dill, and J. L. Dehmer, Pictures of unbound molecular electrons, including shape-resonant states. Eigenchannel contour maps, J. Chem. Phys. **75**, 4546 (1981).
[24] Up to any phase inherited from the initial state (which is spectrally constant).
[25] J. Su, H. Ni, A. Becker, and A. Jaroń-Becker, Numerical simulation of time delays in light-induced ionization, Phys. Rev. A **87**, 033420 (2013).
[26] The phase transferred from the ionizing field amplitude $F(\omega)$ to the EWP according to Eq. (2) is notably exploited in the standard characterization techniques of coherent attosecond XUV pulses [42,43].
[27] A. Chacon, M. Lein, and C. Ruiz, Asymmetry of Wigner's time delay in a small molecule, Phys. Rev. A **89**, 053427 (2014).
[28] J. Wätzel, A. S. Moskalenko, Y. Pavlyukh, and J. Berak-dar, Angular resolved time delay in photoemission, J. Phys. B **48**, 025602 (2015).
[29] W. H. Press, S. A. Teukolsky, W. T. Vetterling, and B. P. Flannery, *Numerical Recipes: The Art of Scientific Computing*, 3rd ed. (Cambridge University Press, New York, 2007).
[30] K. C. Kulander, K. J. Shaffer, and J. L. Krause, Time-dependent studies of multiphoton processes, in *Atoms in Intense Laser Fields*, edited by M. Gavrila (Academic Press, San Diego, CA, 1992), p. 247.
[31] C. J. Joachain, *Quantum Collision Theory*, 3rd ed. (North-Holland, New York, 1983).
[32] A. Messiah, *Quantum Mechanics—Two Volumes Bound as One*, 1st ed. (Dover, Mineola, NY, 1999).
[33] H. A. Bethe and E. E. Salpeter, *Quantum Mechanics of One- and Two-Electron Atoms*, 1st ed. (Plenum, New York, 1977).
[34] J. Cooper and R. N. Zare, Angular distribution of photoelectrons, J. Chem. Phys. **48**, 942 (1968).
[35] A.-T. Le, R. R. Lucchese, and C. D. Lin, Quantitative rescattering theory of high-order harmonic generation for polyatomic molecules, Phys. Rev. A **87**, 063406 (2013).
[36] M. Ya. Amusia, *Atomic Photoeffect* (Plenum, New York, 1990).
[37] T. Carette, J. M. Dahlström, L. Argenti, and E. Lindroth, Multiconfigurational Hartree-Fock close-coupling ansatz: Application to the argon photoionization cross section and delays, Phys. Rev. A **87**, 023420 (2013).
[38] J. M. Dahlström and E. Lindroth, Study of attosecond delays using perturbation diagrams and exterior complex scaling, J. Phys. B **47**, 124012 (2014).
[39] E. S. Toma and H. G. Muller, Calculation of matrix elements for mixed extreme-ultraviolet–infrared two-photon above-threshold ionization of argon, J. Phys. B **35**, 3435 (2002).
[40] M. Vacher *et al.* (unpublished).
[41] V. Gruson *et al.* (unpublished).
[42] P. M. Paul *et al.*, Observation of a train of attosecond pulses from high harmonic generation, Science **292**, 1689 (2001).
[43] M. Hentschel *et al.*, Attosecond metrology, Nature (London) **414**, 509 (2001).